OATAO

Open Archive Toulouse Archive Ouverte

A new intersecting tunnel structure in the $A^I M^{III}[PO_3(OH)]_2$ series for $A^I = Ag$, $M^{III} = In$: Analysis of structural relationships

Anne Guesdon [a,*], Francesca Romero Sarria [b,1], Christophe Tenailleau [a,2], Bernard Raveau [a]

[a] Laboratoire CRISMAT, UMR 6508 CNRS ENSICAEN, Université de Caen Basse-Normandie, 6 Boulevard du Maréchal Juin, 14050 CAEN Cedex, France
[b] Laboratoire Catalyse et Spectrochimie, UMR 6506 CNRS ENSICAEN, 6 Boulevard Maréchal Juin, 14050 CAEN Cedex, France

ABSTRACT

A new indium hydroxyphosphate containing silver, $AgIn[PO_3(OH)]_2$, has been synthesized using hydrothermal method. It crystallizes in the $P2_1/c$ space group with the cell parameters $a = 6.6400(2)$ Å, $b = 14.6269(6)$ Å, $c = 6.6616(4)$ Å, $\beta = 95.681(5)°$, $V = 643.82(6)$ Å^3, $Z = 4$. Its three-dimensional framework, built up of corner-sharing $PO_3(OH)$ tetrahedra and InO_6 octahedra, presents intersecting tunnels running along $<111>$ and $[100]$ directions, in which the Ag^+ cations are located. The presence of hydroxyl groups has been confirmed from IR spectroscopy studies and hydrogen atoms were located from the single crystal X-ray diffraction study. The structural relationships with the other compounds of general formula $A^I M^{III}[PO_3(OH)]_2$ are analyzed.

1. Introduction

Numerous hydroxyphosphates have been explored, either for their protonic conductivity or as precursors for the synthesis of new matrices with microporous properties. The crystal chemistry of these compounds and the rules that govern the formation of their various structures are so far not really understood. In this respect, the hydroxymonophosphates of generic formula $A^I M^{III}[PO_3(OH)]_2$ are of great interest since they form a large family of compounds. To our knowledge, twenty different phosphates with this formula, which can be classified into seven different structural types, have been synthesized to date, with $M(III) =$ In [1–6], V [7,8], Fe [6,9–11] , Al [6,12,13] Ga [6,12] and Sc [14]. These hydroxymonophosphates have been synthesized for univalent cations i.e. alkaline ions from lithium to cesium, and hydroxonium and ammonium cations, showing that the size of the latter plays an important role in the nature of the structural type. This is the case of the indohydroxyphosphates [1–6] for which five structural types can be stabilized, depending on the nature of the of $A(I) =$ Rb, Cs, K, NH_4, Na, Li. Curiously, no silver hydroxyphosphate has been obtained to date in this series. We have thus explored the Ag–In–P–O system using hydrothermal synthesis in order to favour the formation of hydroxyl groups.

We report herein on the synthesis and crystal structure of the silver indohydroxymonophosphate $AgIn[PO_3OH]_2$. We show that this material exhibits an original structure with respect to the previously known hydroxyphosphates with generic formula $AIn[PO_3OH]_2$. A structural analysis of the very rich family $A^I M^{III}[PO_3OH]_2$ is also presented, which demonstrates that the structure of $AgIn[PO_3OH]_2$ exhibits close relationships with those of five other indohydroxymonophosphates with A = Rb, NH_4, K, Na, Li and with the phase $NaSc[PO_3OH]_2$.

2. Experimental

2.1. Crystal synthesis

The single crystal used for the structure determination of $AgIn[PO_3(OH)]_2$ was extracted from a preparation synthesized using hydrothermal method. First, a mixture of 0.1291 g of $AgNO_3$, 0.3165 g of In_2O_3 and 0.5255 g of H_3PO_4 (85%), i.e. corresponding to respective molar ratio 1:1.5:6, was placed in a 21 ml Teflon beaker with 2 ml of deionized water. The initial measured pH was *ca.* 1. The

beaker was covered and placed in a stainless steel Parr autoclave, which was heated up to 220 °C for 36 h. It was then cooled to 120 °C in 20 h and finally brought down to room temperature. The resulting white powder was washed with deionized water and dried in air; it contained as a major phase small colorless crystals of the title compound.

2.2. Crystal studies

The semi-quantitative analysis of a colorless crystal extracted from the preparation was performed with an OXFORD 6650 microprobe mounted on a PHILIPS XL30 FEG scanning electron microscope. It led to the cationic molar composition "23:24:53" for silver, indium and phosphorus, respectively.

Several crystals were then optically selected to be tested. A plate-like single crystal, with approximate dimensions $0.082 \times 0.031 \times 0.034$ mm^3 was chosen for the structure determination and refinement. The data were collected with a Bruker–Nonius Kappa CCD four-circle diffractometer using the Mo Kα radiation, equipped with a bidimensional CCD detector fixed at a distance of 36 mm from the single crystal. A φ and ω scans strategy was determined. Data were collected up to 45° (0.6° per frame, 60 s per degree, 2 iterations). The cell parameters are reported in Table 1. Data were reduced and corrected for Lorentz and polarization effects with the EvalCCD package [15]. Structure determination and refinement were performed with the JANA2000 program [16].

The observed systematic absences $h0l$: $l = 2n + 1$ and $0k0$: $k = 2n + 1$ correspond to the centrosymmetric space group $P2_1/c$ (#14). The structure of AgIn[PO$_3$(OH)]$_2$ was determined using the heavy atom method and successive difference synthesis and Fourier synthesis. Absorption and secondary extinction effect

corrections were applied. In a first step, Ag, In, P and O atoms were localized. The refinement of their atomic coordinates and anisotropic thermal parameters led to the reliability factors $R = 0.0317$ and Rw $= 0.0341$. The maximum of residual electronic densities was then 1.63 e Å^{-3}. The chemical formula for the cell content deduced from this refinement, "AgIn(PO$_4$)$_2$", suggested that two positive charges per formula unit were missing to ensure the charge balance. Bond valence sum (BVS) calculations [17] were performed at this stage of the refinement. The calculated values for silver, indium, phosphorus cations and O(1), O(2), O(4), O(5) oxygen anions were close to the theoretical values of 1, 3, 5 and 2, respectively. For O(3) and O(6), a slight lack of valence was observed (respective BVS values of 1.82 and 1.78) and O(7) and O(8) presented respective BVS values of 1.28 and 1.10. These calculations suggested the presence of two hydrogen atoms linked to O(7) and O(8) and forming hydrogen bonds with O(3) and O(6). In order to localize the corresponding hydrogen atoms, difference Fourier maps were calculated with reflections of low θ diffraction angles (from 5° to about 20°). From their examination, two hydrogen atoms H(1) and H(2) linked to O(7) and O(8), respectively, could be localized.

The resulting chemical formula was thus AgIn[PO$_3$(OH)]$_2$ ($Z = 4$), for which charge balance is respected. The final refinement of atomic coordinates for all atoms (including hydrogen atoms), with anisotropic displacement parameters for Ag, In, P and O atoms and isotropic displacement parameters for hydrogen atoms, led to reliability factors $R = 0.0314$ and Rw $= 0.0332$ (Table 1). The atomic coordinates, equivalent isotropic thermal parameters and their estimated standard deviations are listed in Table 2. The distances and angles, including O–H⋯O bonds and angles, are given in Table 3. The BVS calculations performed after the insertion of hydrogen atoms H(1) and H(2) are in agreement with the expected values for Ag, In, P, O and H atoms (Table 4).

Further details of the crystal structure investigations (including the anisotropic thermal parameters) can be obtained from the Fachinformationszentrum Karlsruhe, 76344 Eggenstein-Leopoldshafen, Germany, (fax: (49) 7247 808 666; e-mail: crysdata@fiz-karlsruhe.de) on quoting the depository number CSD-418327.

2.3. Polycrystalline powder sample studies

2.3.1. Synthesis

The silver indium hydroxyphosphate AgIn[PO$_3$(OH)]$_2$ was synthesized in the form of a monophasic polycrystalline powder sample using the following procedure. First, 0.4281 g of AgNO$_3$, 0.3499 g of In$_2$O$_3$ and 0.6656 g of (NH$_4$)$_2$HPO$_4$ were mixed in an

Table 1
Summary of crystal data, intensity measurements and structure refinement parameters for AgIn[PO$_3$(OH)]$_2$.

1 – Crystal data	
Crystal dimensions (mm^3)	$0.082 \times 0.031 \times 0.034$
Space group	$P2_1/c$
Cell dimensions	$a = 6.6400(2)$ Å
	$b = 14.6269(6)$ Å
	$c = 6.6616(4)$ Å
	$\beta = 95.680(5)°$
Volume	643.82(5) Å^3
Z	4
Formula weight (g mol^{-1})	414.6
ρcalc (g cm^{-3})	4.2765
2 – Intensity measurements	
λ(Mo Kα)	0.71069 Å
Scan strategies	φ and ω scans
	0.6°/frame
	60 s/°
	2 iterations
Crystal-detector distance	Dx = 36 mm
θ range for data collection	$5.88° \leq \theta \leq 45°$
Limiting indices	$-12 \leq h \leq 13$
	$-27 \leq k \leq 29$
	$-12 \leq l \leq 13$
Measured reflections	24,598
Reflections with $I > 3\sigma$	5294
Independant reflections with $I > 3\sigma$	3254
μ(mm^{-1})	7.127
Extinction coefficient g (type I, Gaussian isotropic)	0.23(2)
3 – Structure solution and refinement	
Parameters refined	118
Agreement factors	$R = 0.0314$
	$R_w = 0.0332$
Weighting scheme	$w = 1/(\sigma^2(F) + 4.10^{-4}F^2)$
Δ/σ max	1.81×10^{-2}

Table 2
Positional parameters and their estimated standard deviations in AgIn[PO$_3$(OH)]$_2$.

Atom	x	y	z	U (Å^2)
Ag	0.20835(4)	−0.068103(17)	−0.01701(3)	0.02354(6)
In	0.76767(2)	0.607603(10)	0.12190(2)	0.00638(3)
P(1)	0.72624(9)	0.84477(4)	0.11857(9)	0.00718(13)
P(2)	0.75173(9)	0.38428(4)	0.00377(9)	0.00756(13)
O(1)	0.7416(3)	0.46358(12)	0.1517(3)	0.0124(4)
O(2)	1.0917(3)	0.59943(13)	0.1465(3)	0.0109(4)
O(3)	0.4534(3)	0.63884(14)	0.1078(3)	0.0141(5)
O(4)	0.7993(3)	0.59959(12)	0.4452(3)	0.0124(4)
O(5)	0.7599(3)	0.59758(12)	−0.1932(3)	0.0143(5)
O(6)	0.8306(3)	0.75226(12)	0.1456(3)	0.0136(4)
O(7)	0.4924(3)	0.82823(15)	0.0666(3)	0.0175(5)
O(8)	0.8053(3)	0.29442(14)	0.1288(3)	0.0150(5)
H(1)	0.464(8)	0.781(4)	0.066(9)	0.061(18)
H(2)	0.893(8)	0.283(4)	0.166(9)	0.046(16)

The atomic displacement parameters of hydrogen atoms were refined isotropically (U_{iso}). The atomic displacement parameters of all other atoms were refined anisotropically and are given in the form of an equivalent isotropic displacement parameter defined by $U_{eq} = 1/3 \sum_{i=1}^{3} \sum_{j=1}^{3} U_{ij} a^{*i} a^{*j} \vec{a}_i \vec{a}_j$.

Table 3
Distances (Å) and angles (°) in AgIn[PO$_3$(OH)]$_2$.

In	O(1)	O(2)	O(3)	O(4)	O(5)	O(6)
O(1)	**2.1246(18)**	3.061(3)	3.195(3)	2.789(2)	3.031(3)	4.264(3)
O(2)	91.60(7)	**2.1452(17)**	4.260(2)	2.914(3)	2.998(2)	2.829(3)
O(3)	97.38(7)	170.63(7)	**2.1289(17)**	3.104(2)	3.055(3)	2.994(3)
O(4)	81.54(7)	85.55(7)	93.10(7)	**2.1463(17)**	4.235(2)	3.016(3)
O(5)	91.71(7)	89.88(7)	92.52(8)	171.73(7)	**2.0994(18)**	3.197(3)
O(6)	168.99(7)	82.15(7)	88.56(7)	88.91(7)	97.30(7)	**2.1596(18)**

P(1)	O(4^i)	O(5^{ii})	O(6)	O(7)
O(4^i)	**1.5306(19)**	2.449(3)	2.543(3)	2.500(3)
O(5^{ii})	107.34(10)	**1.5095(19)**	2.510(3)	2.516(3)
O(6)	112.78(11)	111.71(11)	**1.5229(19)**	2.515(3)
O(7)	107.15(11)	109.27(12)	108.47(11)	**1.576(2)**

P(2)	O(1)	O(2^{iii})	O(3^{iv})	O(8)
O(1)	**1.5277(19)**	2.541(3)	2.543(3)	2.517(3)
O(2^{iii})	112.31(10)	**1.5315(19)**	2.508(2)	2.548(3)
O(3^{iv})	112.88(11)	110.32(10)	**1.5240(18)**	2.419(3)
O(8)	108.30(11)	110.04(11)	102.51(11)	**1.578(2)**

	O–H	O–H$\cdots$O	H$\cdots$O
O(7)–H(1)–O(3)	0.72(5)	165(6)	2.09(5)
O(8)–H(2)–O(6^v)	0.63(5)	168(7)	2.17(5)

Ag – O(1^{vi}) = 2.4673(18).
Ag – O(2^{vii}) = 2.3429(17).
Ag – O(4^{vi}) = 2.5006(18).
Ag – O(4^{vii}) = 2.7417(19).
Ag – O(7^{viii}) = 2.441(2).
Symmetry codes:
i: x; $3/2 - y$; $-1/2 + z$.
ii: x; $3/2 - y$; $1/2 + z$.
iii: $2 - x$; $1 - y$; $-z$.
iv: $1 - x$; $1 - y$; $-z$.
v: $2 - x$; $1 - y$; $1/2 - z$.
vi: $1 - x$; $-1/2 + y$; $1/2 - z$.
vii: $-1 + x$; $1/2 - y$; $-1/2 + z$.
viii: x; $-1 + y$; z.

agate mortar (according to the stoichiometric proportions, i.e. with respective molar ratio 1:0.5:2). The finely ground mixture was placed in a platinum crucible and heated in air at 400 °C in order to eliminate nitrogen oxides, ammonia and water molecules. Once the correct weight loss was reached, the resulting mixture was ground again and placed with 1 ml of deionized water in a 21 ml Teflon-lined stainless steel Parr autoclave. It was heated up to 220 °C for 24 h, then cooled down to 120 °C in 10 h and finally brought back to room temperature. The resulting product was washed with deionized water and dried in air. The purity of the resulting white powder sample was checked from a powder X-ray diffraction pattern registered from $2\theta = 5°$ to $100°$ (λ(Cu Kα)) using a Philips Xpert Pro diffractometer.

2.3.2. Thermogravimetric analysis

The presence of hydroxyl groups in the title compound was checked by thermogravimetry, using a TGA 92-16.18 Setaram

microbalance. In a first time, 17 mg of the powder sample were placed in a platinum crucible in air and heated in the microbalance at 100 °C for 1 h in order to remove the eventually physisorbed water. The sample was then heated up to 400 °C at 1 °C/min.

A weight loss of 4.28% was observed between 300 and 350 °C, in agreement with the theoretical value expected for the departure of one water molecule per formula unit (4.34%).

2.3.3. Infra-red spectroscopy studies

The IR skeletal spectra have been recorded in the region above 400 cm^{-1} by diluting 20% of the sample powder in KBr pressed disks (10 mg cm^{-2}), using a Nicolet Magna 550 Fourier transform instrument equipped with a KBr beam splitter and with a DTGS

Table 4
Valence calculations in AgIn[PO$_3$(OH)]$_2$.

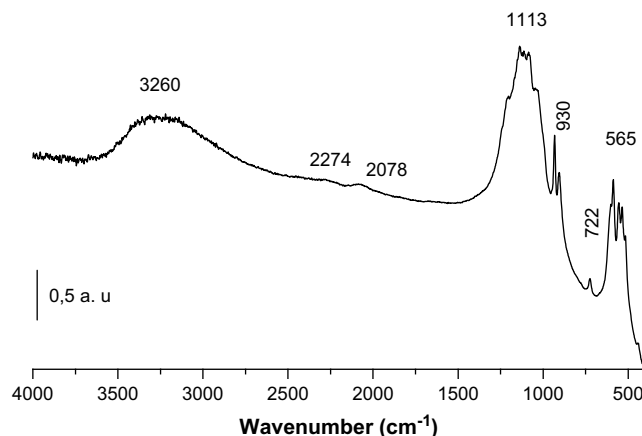|	Ag	In	P(1)	P(2)	$\Sigma\nu_i$	H(1)	H(2)	$\Sigma\nu_i$
O(1)	0.167	0.548		1.266	**1.981**			**1.981**
O(2)	0.234	0.518		1.253	**2.005**			**2.005**
O(3)		0.542		1.279	*1.820*	0.198		**2.019**
O(4)	0.153	0.517	1.256		**2.005**			**2.005**
	0.080							
O(5)		0.586	1.330		**1.916**			**1.916**
O(6)		0.498	1.283		*1.781*		0.182	**1.963**
O(7)	0.179		1.111		*1.290*	0.852		**2.142**
O(8)				1.105	*1.105*		0.937	**2.042**
$\Sigma\nu_i$	**0.812**	**3.209**	**4.980**	**4.903**		**1.050**	**1.119**	

The bold values correspond to the bond valence sums; the values showing a lack of valence before the insertion of hydrogen atoms in the structure are in italic.

Fig. 1. FTIR spectrum of AgIn[PO3(OH)]2 in KBr (20% sample).
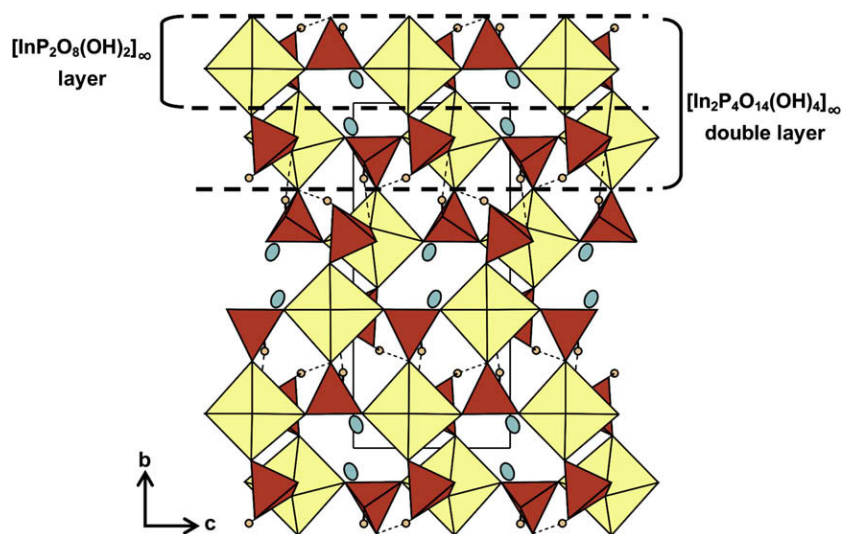
Fig. 2. Projection of the structure of AgIn[PO$_3$(OH)]$_2$ along [100].
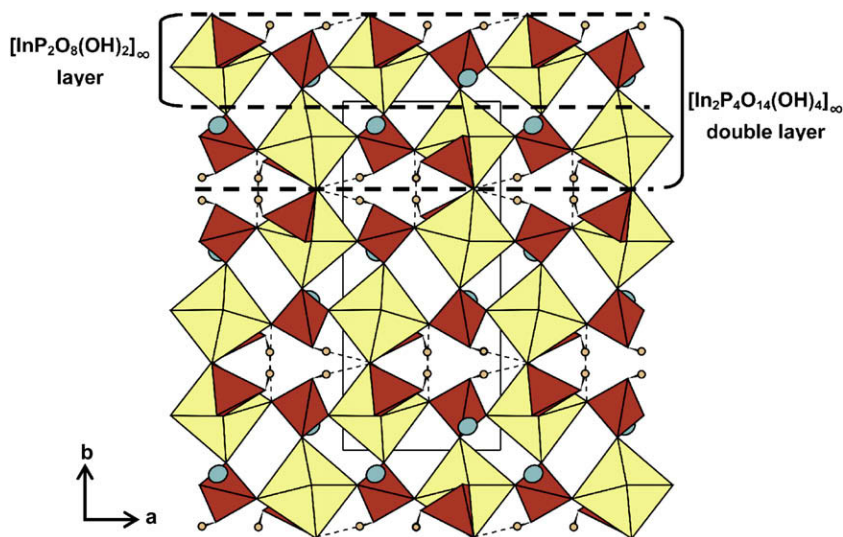
Fig. 3. Projection of the structure of AgIn[PO$_3$(OH)]$_2$ along [001].
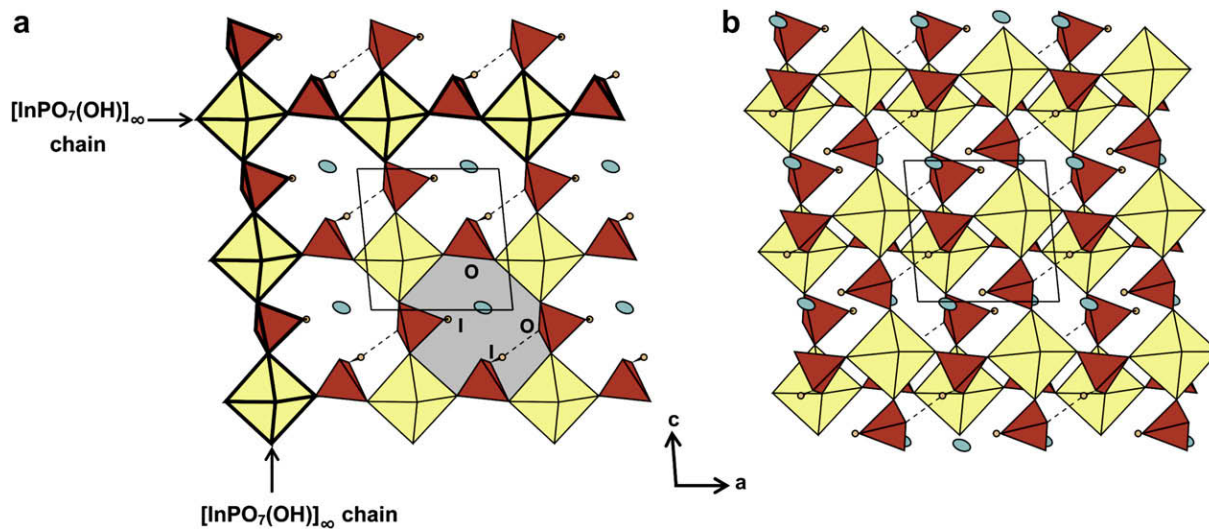
Fig. 4. a) Projection along [010] of one [InP$_2$O$_8$(OH)$_2$]$_\infty$ layer parallel to (010), showing the [InPO$_7$(OH)]$_\infty$ chains running along [100] and [001]. (b) Projection along [010] of one [In$_2$P$_4$O$_{14}$(OH)$_4$]$_\infty$ double-layer resulting from the connection along $\vec{b}$ of two enantiomorphic [InP$_2$O$_8$(OH)$_2$]$_\infty$ layers.

Table 5
Structural features of the $A^I M^{III}[PO_3(OH)]_2$ compounds.

Structural features		$A^I M^{III}$	References	SG	a	b	c	α	β	γ	V	Z	V/Z
I $M_3O_6[PO_3(OH)_6]$ units	Triclinic	(α-)CsIn	[6]	P-1	7.4146	9.0915	9.7849	65.525	70.201	69.556	547.77	3	182.59
		α-RbV	[7]	P-1	8.831	9.45	7.188	109.55	110.26	65.34	498.54	3	166.18
		(α-)NH₄V	[8]	P-1	7.173	8.841	9.458	65.08	70.68	69.59	497.73	3	165.91
		NH₄(Al₀.₆₄Ga₀.₃₆)	[12]	P-1	7.109	8.695	9.252	65.01	70.25	69.01	472.04	3	157.35
		H₃OAl	[13]	P-1	7.1177	8.6729	9.22	65.108	70.521	68.504	469.42	3	156.47
		NH₄Fe	[10]	I-1	9.838	7.185	14.159	93.46	85.58	89.47	995.95	6	165.99
		α-RbFe	[6]	P-1	7.2025	8.8329	9.454	65.149	70.045	69.951	497.44	3	165.81
	Trigonal	RbAl	[6]	R-3c	8.0581	8.0581	51.081	90	90	120	2872.5	18	159.58
		RbGa	[6]	R-3c	8.1188	8.1188	51.943	90	90	120	2965.1	18	164.73
		RbFe	[11]	R-3c	8.16	8.16	52.75	90	90	120	3041.82	18	168.99
II $[M_2(PO_3(OH))_6]_\infty$ ribbons		β-RbV	[7]	P2₁/c	5.21	8.789	14.33	90	94.39	90	654.26	4	163.57
		(β-)NH₄V	[7]	P2₁/c	5.201	8.738	14.398	90	94.83	90	652	4	163.00
		H₃OFe	[9]	P2₁/c	5.191	8.748	14.448	90	94.81	90	653.79	4	163.45
		CsIn-	[5]	P2₁/c	5.3286	9.1653	14.7839	90	93.849	90	720.39	4	180.10
III $[MP_2O_8(OH)_2]_\infty$ layers	I–I–O–O	NaSc	[14]	Cc	10.4446	16.371	9.0553	90	122.42	90	1307.02	8	163.38
	I–O–I–O	KIn	[3]	P2₁/c	9.6232	8.2573	9.4571	90	115.72	90	677.03	4	169.26
		NH₄In	[3-4]	P2₁/c	9.6651	8.2763	9.5964	90	116.15	90	689.06	4	172.27
		RbIn	[3]	P2₁/c	9.705	8.367	9.528	90	116.6	90	691.8	4	172.95
	I–I–I–O and O–O–O–I	NaIn	[2]	P-1	9.30131	9.4976	9.2685	98.71	98.953	60.228	699.42	4	174.86
	I–O–I–O	LiIn	[1]	Pmnn	5.49	7.946	6.929	90	90	90	302.27	2	151.14
	I–I–O–O	AgIn	[This work]	P2₁/c	**6.64**	**14.6269**	**6.6616**	**90**	**95.68**	**90**	**643.82**	**4**	**160.96**

detector. Sample was treated under vacuum in a classical quartz cell, and spectra were recorded (resolution $4\ cm^{-1}$) at room temperature.

The obtained spectrum is shown in Fig. 1. Two groups of bands can be distinguished: in $1300–800\ cm^{-1}$ and $700–400\ cm^{-1}$ regions. According to literature data, the first set of bands may be attributed to asymmetric and symmetric stretches of P–O bonds, and the second to the bending vibrations [18]. The features appearing in $2300–2000\ cm^{-1}$ are probably due to combination bands of phosphates [19]. In the high frequencies region, a broad band centered at $3260\ cm^{-1}$ is observed. When water is present in a solid structure, the ν(OH) is detected between 3300 and $3400\ cm^{-1}$ and the $\delta(H_2O)$ appears around $1600–1620\ cm^{-1}$ [20]. In our case, no bands in the $\delta(H_2O)$ region are detected. Therefore, we can say that there are no water molecules in the structure but hydroxyl groups linked through hydrogen bonds to the oxygen atoms of the framework.

3. Description of the structure

The 3D-framework of $AgIn[PO_3(OH)]_2$ is built from corner-sharing InO_6 octahedra and PO_3OH tetrahedra and, as shown in Figs. 2 and 3, it can easily be described as a stacking along $\vec{b}$ of $[InP_2O_8(OH)_2]_\infty$ layers parallel to (010). In these layers, which result from the intercrossing of $[InPO_7(OH)]_\infty$ chains parallel to the [100] and [001] directions (Fig. 4a), each InO_6 octahedron is linked to four $PO_3(OH)$ tetrahedra (two P(1) and two P(2)) whereas each tetrahedron is linked to two InO_6 octahedra. As a result, quite large 8-sided windows delimited by four InO_6 octahedra and four $PO_3(OH)$ tetrahedra is observed in the $[InP_2O_8(OH)_2]_\infty$ layers (Fig. 4a). Along the [010] direction, two enantiomorphic $[InP_2O_8(OH)_2]_\infty$ layers are connected to form $[In_2P_4O_{14}(OH)_2]_\infty$ double-layers parallel to (010), the In octahedron of one layer sharing one apex with a P(2) tetrahedron of the enantiomorphic layer (Figs. 2 and 3 and Fig. 4b). Finally, the $[InP_2O_6(OH)_2]_\infty$ host-lattice results from the assembly along $\vec{b}$ of two $[In_2P_4O_{14}(OH)_2]_\infty$ double-layers, deduced one from the other through a c glide mirror (Figs. 2 and 3). Here again, the InO_6 octahedra of one double-layer share one corner with a P(1) hydroxymonophosphate group of the other double-layer. The resulting three-dimensional framework presents tunnels running along the [100], [001] and <111> directions. The silver cations sit in the previously

mentioned windows lying in the $[InP_2O_8(OH)_2]_\infty$ layers (Fig. 4a) and are thus located at the intersections of the tunnels running along <111> and [100] (Fig. 2). Each silver cation is surrounded by four oxygen atoms and one hydroxyl group forming a distorted trigonal bipyramid. The Ag–O distances are ranging from
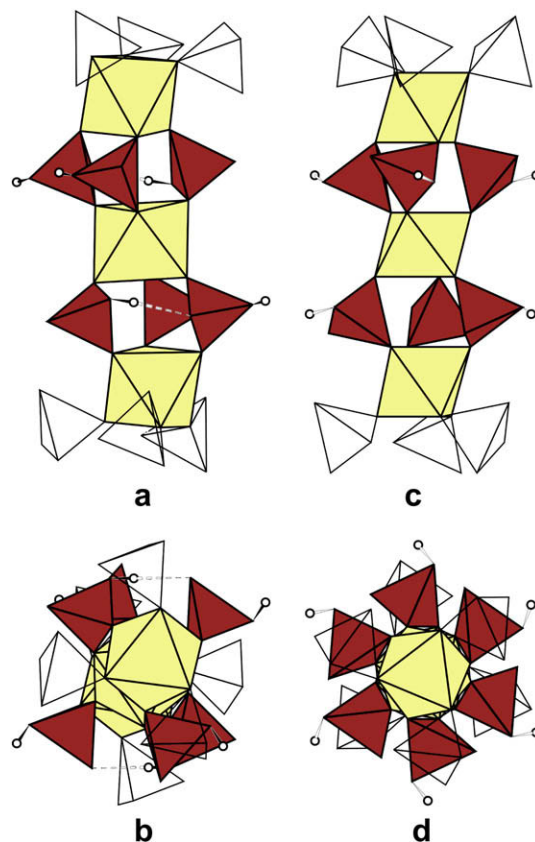

Fig. 5. Projections of one $M_3O_6[PO_3(OH)_6]$ structural unit in the triclinic structure type (a and b) and in the trigonal structure type (c and d) of $A^I M^{III}[PO_3(OH)]_2$ compounds, showing the different relative orientation of the polyhedra and especially of the tetrahedra in the two framework types. The white tetrahedra correspond to the hydroxymonophosphate groups belonging to adjacent $M_3O_6[PO_3(OH)_6]$ structural units.
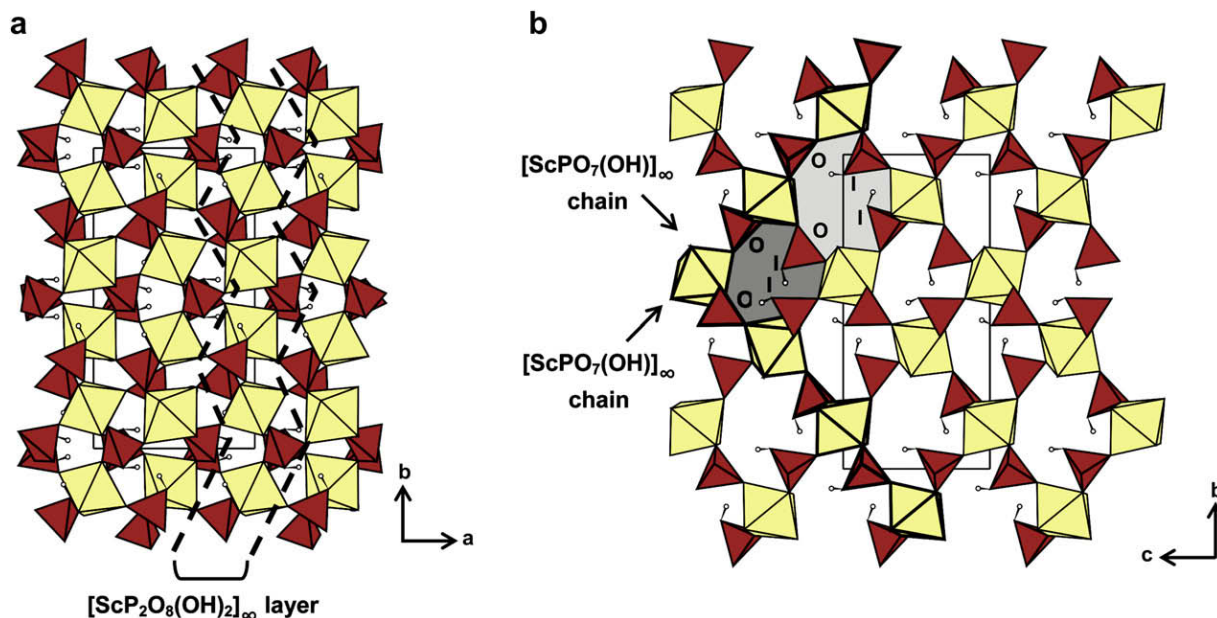
Fig. 6. The monoclinic structure type of NaSc[PO$_3$(OH)]$_2$. (a) Projection along [001] of the structure of NaSc[PO$_3$(OH)]$_2$. One [ScP$_2$O$_8$(OH)$_2$]$_\infty$ layer has been underlined. (b) Projection along [100] of one [ScP$_2$O$_8$(OH)$_2$]$_\infty$ layer, showing the intercrossed [ScPO$_7$(OH)]$_\infty$ chains, the two types of 8-sided windows (highlighted in grey) and the "I–I–O–O" sequences of the hydroxyl groups in these windows.

2.3429(17) Å to 2.7417(19) Å (Table 3). The InO$_6$ octahedra are quite regular, with six In–O bonds ranging from 2.0994(18) Å to 2.1596(18) Å (mean In–O distance: 2.134 Å), i.e. in agreement with the values given in literature for InO$_6$ octahedra sharing their six corners with phosphate groups (see for instance Refs. [1–4,21,22]). Both P(1) and P(2) tetrahedra present three P–O distances comprised between 1.5095(19) Å and 1.5315(19) Å and one larger bond of 1.576(2) Å for P(1)–O(7) and 1.578(2) Å for P(2)–O(8). This is the geometry usually observed for hydroxymonophosphate groups, in which the larger distance corresponds to the P–OH bond (see for instance Refs. [2,4,6,8,9,14]).

4. Discussion

The A^{I}M^{III}[PO$_3$(OH)]$_2$ compounds form a very rich family: to our knowledge, 20 compounds, corresponding to 7 different structural types, have been reported up to date with this general formula (Table 5). AgIn[PO$_3$(OH)]$_2$ is thus the 21st compound of this family and it exhibits a new structure type. All these hydroxyphosphates consist of corner-sharing M^{III}O$_6$ octahedra and PO$_3$(OH) groups, and we will show that several of them present close relationships. Three groups of structural types can be distinguished depending on the polyhedral arrays encountered in the [M^{III}[PO$_3$(OH)]$_2$]$_\infty$ frameworks (Table 5).

The first group (I) corresponds to two structure types, which are both built up from M$_3$O$_6$[PO$_3$(OH)$_6$] basic units:

(i) The most frequently observed framework corresponds to α-CsIn- [6], α-RbV- [7], α-NH$_4$V- [8], NH$_4$(Al$_{0.64}$Ga$_{0.36}$)- [12], H$_3$OAl- [13], NH$_4$Fe- [10] and α-RbFe- [6] compounds, which crystallize with a triclinic symmetry. In this structure type, the 3D host-lattice presents numerous intersecting tunnels. It is built from M$_3$O$_6$[PO$_3$(OH)$_6$] basic units resulting from the connection of three MO$_6$ octahedra with six monophosphate groups through corner sharing (Fig. 5a–b).

(ii) Similar M$_3$O$_6$[PO$_3$(OH)$_6$] units are encountered in the second structure type, which actually presents very close relationships with the former one. The topology of the structure of RbAl- [6],
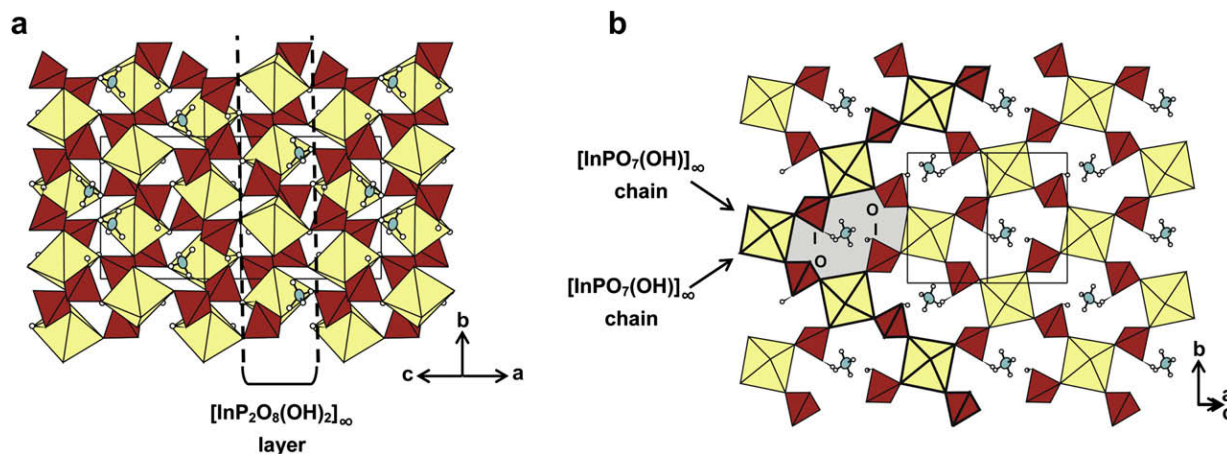

Fig. 7. The monoclinic structure type of A^{I}M^{III}[PO$_3$(OH)]$_2$ compounds (KIn, NH$_4$In, RbIn). (a) Projection along [101] of the structure of NH$_4$In[PO$_3$(OH)]$_2$. One [InP$_2$O$_8$(OH)$_2$]$_\infty$ layer has been underlined. (b) Projection along [$\bar{1}$01] of one [InP$_2$O$_8$(OH)$_2$]$_\infty$ layer, showing the intercrossed [InPO$_7$(OH)]$_\infty$ chains and the "I–O–I–O" sequence of the hydroxyl groups in a 8-sided window.
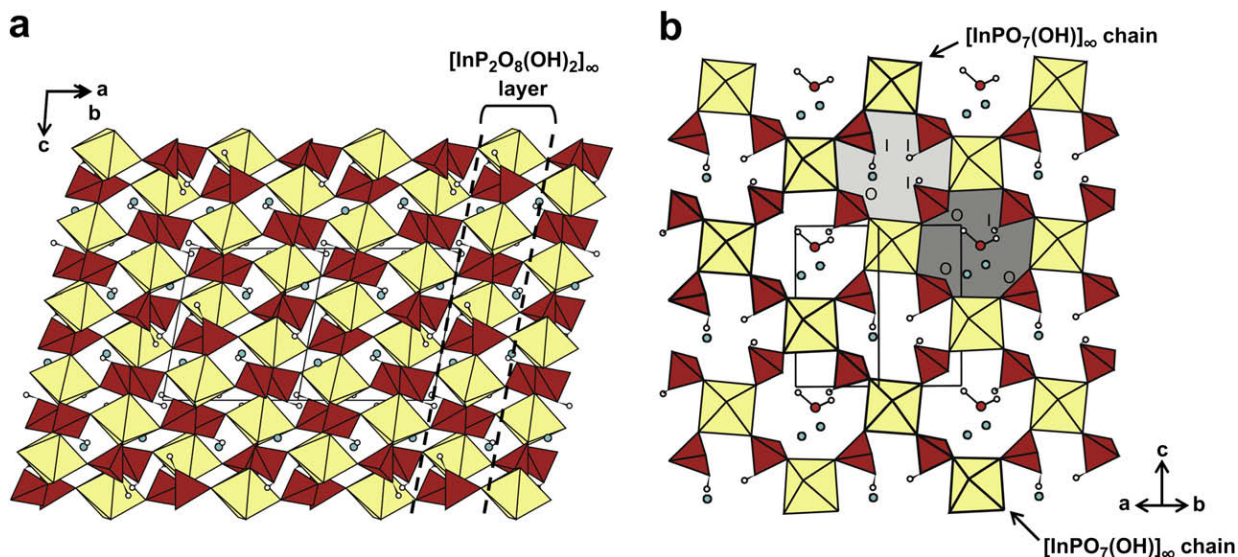
Fig. 8. The triclinic structure type of NaIn[PO$_3$(OH)]$_2$. (a) Projection along[$\bar{1}$10] of the structure. One [InP$_2$O$_8$(OH)$_2$]$_\infty$ layer has been underlined. (b) Projection along [110] of one [InP$_2$O$_8$(OH)$_2$]$_\infty$ layer, showing the the intercrossed [InPO$_7$(OH)]$_\infty$ chains and the "I–I–I–O" and "O–O–O–I" sequences of the hydroxyl groups in the two kinds of 8-sided windows.

RbGa- [6] and RbFe- [11] compounds is indeed the same as that of the first type, but the relative orientation of the polyhedra (and thus of the hydroxyl groups) is slightly different, corresponding to a higher symmetry of the structure (trigonal) (Fig. 5c–d).

The hydroxyphosphates of the second group (II), β-RbV- [7], β-NH$_4$V- [7], CsIn [5] and H$_3$OFe- [9], present a monoclinic symmetry and their 3D-framework, contrary to the two previous structure types, does not exhibits intersecting tunnels but only one large elliptic tunnel containing the monovalent cation.

The third group (III) exhibits, with the discovery of AgIn[-PO$_3$(OH)]$_2$, five structural types which are closely related to each other. All these hydroxyphosphates present 3D-frameworks resulting from the stacking of [MP$_2$O$_8$(OH)$_2$]$_\infty$ layers. However, the comparison of these layers reveals different relative orientations of the polyhedra, which induce different connection modes of the

layers and explain that different structure types are observed. This may be evidenced by comparing the size and the shape of the 8-sided windows (delimited by 4 octahedra and four hydroxymonophosphate groups) lying in the [MP$_2$O$_8$(OH)$_2$]$_\infty$ layers. In order to analyze the structural differences of the [MP$_2$O$_8$(OH)$_2$]$_\infty$ layers in the different structure types, we have chosen to compare the orientation of the four hydroxyl groups of the PO$_3$OH tetrahedra which delimit, with four MO$_6$ octahedra, a given 8-sided window. The following notation will be used: an hydroxyl group pointing towards the inside of the considered window will correspond to the letter "I", whereas if the OH group points towards the outside of the window it will be indicated by the letter "O". A given window will thus be described by a sequence of 4 letters ("I" or "O").

(i) In the NaSc-phase [14], two kinds of windows can be distinguished in the [MP$_2$O$_8$(OH)$_2$]$_\infty$ layers of the monoclinic 3D-framework, one being larger than the other (Fig. 6).

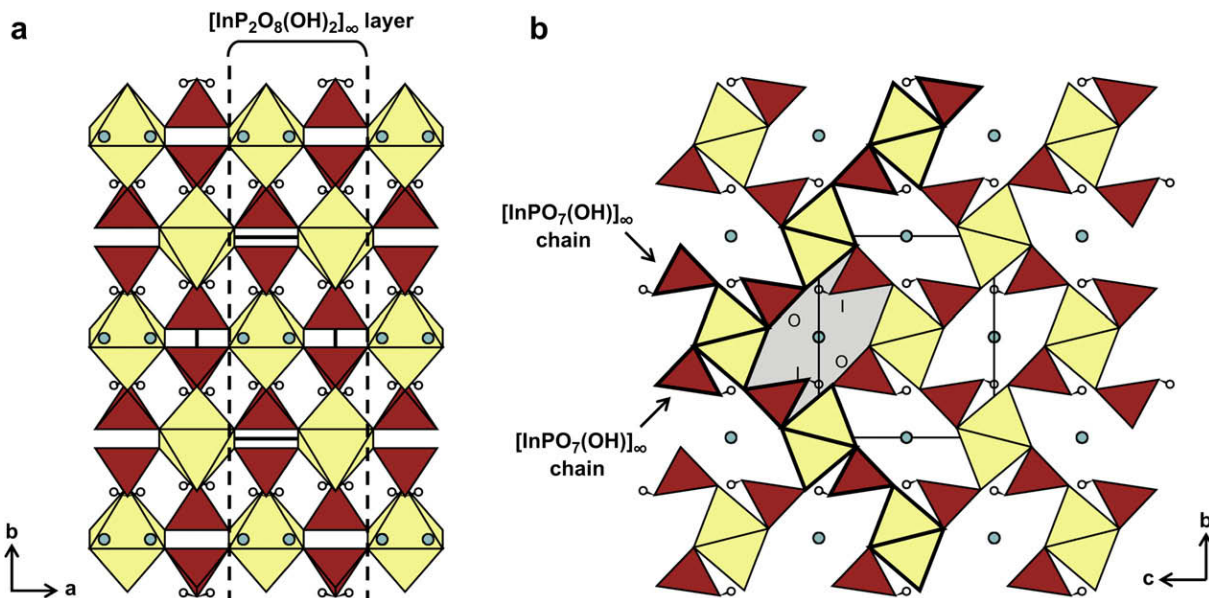**Fig. 9.** The orthorhombic structure type of LiIn[PO$_3$(OH)]$_2$. (a) Projection along [001] of the structure. One [InP$_2$O$_8$(OH)$_2$]$_\infty$ layer has been underlined. (b) Projection along [100] of one [InP$_2$O$_8$(OH)$_2$]$_\infty$ layer, showing the the intercrossed [InPO$_7$(OH)]$_\infty$ chains and the "I–O–I–O" sequence of the hydroxyl groups in a 8-sided window.
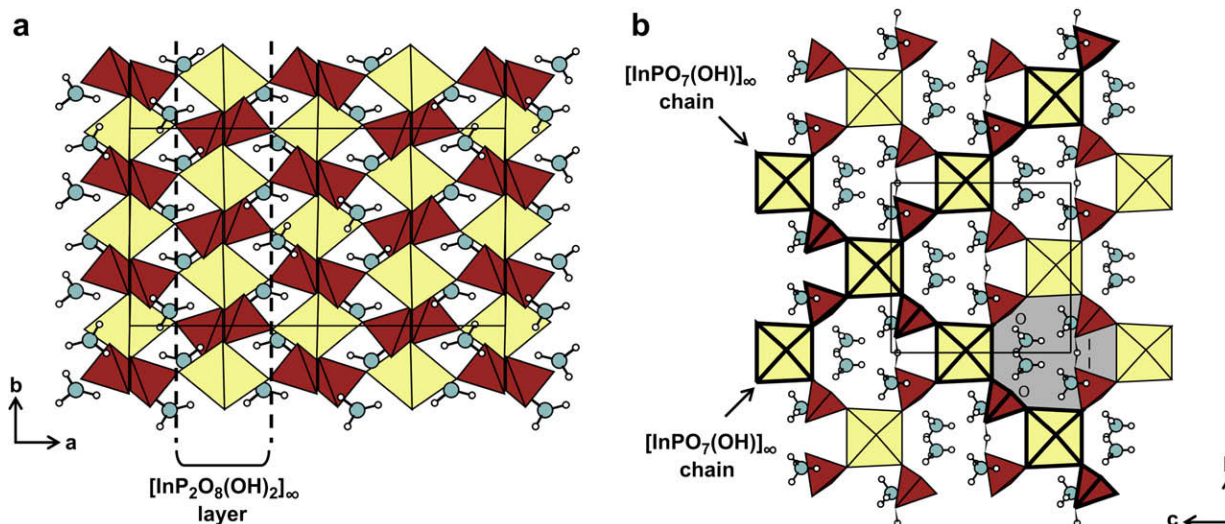
Fig. 10. The orthorhombic structure of (NH₄)₂In[PO₄(HPO₄)]. (a) Projection along [001] of the structure. One [InP₂O₉(OH)]∞ layer has been underlined. (b) Projection along [100] of one [InP₂O₉(OH)]∞ layer, showing the the intercrossed [InPO₇(OH)]∞ chains and the "I–I–O–O" sequence of the hydroxyl groups in a 8-sided window.

However, both present the same "hydroxyl groups sequence": "I–I–O–O".

(ii) The RbIn- [3], NH₄In- [3,4] and KIn- [3] hydroxymonophosphates also crystallize with a 3D-monoclinic structure, but there is only one kind of window in the [InP₂O₈(OH)₂]∞ layers. As for the previous structure, two hydroxyl groups out of four are directed towards the inside of the windows (Fig. 7) but with a different sequence: "I–O–I–O".

(iii) The substitution of Rb⁺, NH₄⁺ or K⁺ by Na⁺ in the [In(PO₃OH)₂]∞ host-lattice is going with the insertion of water molecules in the tunnels [2]. It induces a distortion of the framework leading to a triclinic structure for Na₂In₂[PO₃(OH)]₄·H₂O. A different orientation of the tetrahedra in regard with the octahedra is observed in the [InP₂O₈(OH)₂]∞ layers, leading to the existence of two types of 8-sided windows alternating along the [101] direction (Fig. 8). For the smallest of these windows type, three hydroxyl groups out of

four are pointing towards the center of the window ("I–I–I–O"), whereas the other type of windows is quite larger, since only one hydroxyl group is directed towards its center ("O–O–O–I").

(iv) The insertion of lithium in the [InP₂O₆(OH)₂]∞ framework leads to an orthorhombic structure [1], based on the same structural arrangements, but with a different configuration of the polyhedra (Fig. 9). One can indeed notice that, in this structure, the intercrossed [InPO₇OH]∞ chains which constitute the [InP₂O₈(OH)₂]∞ layer are of two different types. Along the [011] direction, the two oxygen atoms shared between one octahedron and two hydroxymonophosphate groups correspond to adjacent apices of the InO₆ octahedron, whereas along the [01$\bar{1}$] direction (as in all other [InP₂O₈(OH)₂]∞ layer types observed for A^{I}M^{III}[PO₃(OH)]₂ compounds) they correspond to opposite apices of the InO₆ octahedron. All the 8-sided windows lying in the [InP₂O₈(OH)₂]∞ layers have
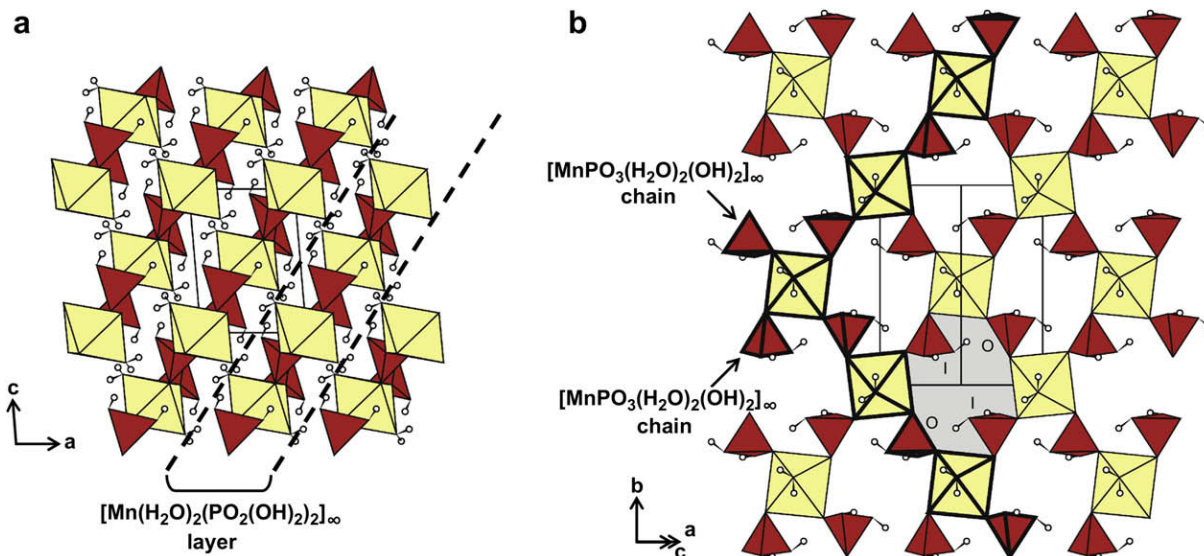
Fig. 11. The monoclinic 2D-structure of M(H₂PO₄)₂(H₂O)₂ compounds (M = Mn, Cd, Zn). (a) Projection along [010] of the structure of Mn(H₂PO₄)₂(H₂O)₂. One [Mn(H₂O)₂(PO₂(OH)₂)₂]∞ layer has been underlined. (b) Projection along [$\bar{1}$01] of one [Mn(H₂O)₂(PO₂(OH)₂)₂]∞ layer, showing the the intercrossed [MnPO₃(H₂O)₂(OH)₂]∞ chains and the "I–O–I–O" sequence of the hydroxyl groups in a 8-sided window.

similar shapes, rather elongated, with two OH groups out of four pointing inside the window, corresponding to the sequence "I–O–I–O".

(v) Finally, in the structure of the title-compound AgIn-, the sequence for the hydroxyl groups is "I–I–O–O" (Fig. 4a), i.e. similar to that encountered in the NaSc-phase (Fig. 6), but with a much more regular shape of the windows of the $[InP_2O_8(OH)_2]_\infty$ layers.

One can notice that $[MP_2O_8(OH)_2]_\infty$ layers similar to that encountered in the five last $A^IM^{III}[PO_3(OH)]_2$ structure types have often been observed in metal phosphates, as for instance in the vanadium phosphates $SiVO(PO_4)_2$ [23,24], $Pb_2(VO)$ $(V_2P_4O_{16})$ [25], or $LiVP_2O_7$ [26]. However, in the latter compounds, the whole framework cannot be described exclusively from these layers. It appears thus more interesting to make structural comparisons with the orthorhombic structure of $(NH_4)_2In[(PO_4)H(PO_4)]$ [27], which is exclusively built up from $[InP_2O_9(OH)]_\infty$ layers, very similar to the $[MP_2O_8(OH)_2]_\infty$ ones. As shown in Fig. 10, the main difference between the $[InP_2O_9(OH)]_\infty$ layers of $(NH_4)_2In[(PO_4)H(PO_4)]$ and the $[InP_2O_8(OH)_2]_\infty$ layers, observed for instance in $(NH_4)In[PO_3(OH)]_2$ (Fig. 7), comes from the presence of one hydrogen atom shared between two phosphates groups. This dictates the config-uration of the hydroxyl groups, leading to the sequence "I–I–O–O" (versus "I–O–I–O" for $(NH_4)In[PO_3(OH)]_2$).

To achieve this structural analysis, the 2D-structure of the $M(H_2PO_4)_2(H_2O)_2$ compounds (M = Mn, Cd, Zn) [28–30] has to be examined, since it consists of $[M(H_2O)_2(PO_2(OH)_2)_2]_\infty$ layers which topology very similar to that of the $[MP_2O_8(OH)_2]_\infty$ layers described above (Fig. 11). Only one type of 8-sided window is present, corresponding to an hydroxyl group sequence "I–O–I–O", i.e. similar to that observed for the NH₄In-structure type but, once again with a different relative orientation of the octahedra and tetrahedra.

5. Conclusion

These structural comparisons emphasize the richness of the $A^IM^{III}[PO_3(OH)]_2$ family of compounds. Concerning the structure types involving $[InP_2O_8(OH)_2]_\infty$ layers, an evolution of the indo-phosphate framework and of its symmetry can be directly related to the size of the A^+ inserted cation. However, it appears difficult to establish an obvious rule which would indicate, according to the nature of both A^I and M^{III} cations, with which type of framework a compound of this family would crystallize. Further explorations of "A–M–P–O–H" systems at the $A^IM^{III}[PO_3(OH)]_2$ composition will probably lead to isolate new phases in this family. They may also lead to new structural types for these compounds, allowing a better understanding of the influence of the size and nature of A^I and M^{III} cations, but also of the synthesis conditions, on the resulting framework.

References

[1] O.A. Gurbanova, E.L. Belokoneva, O.V. Dimitrova, A.G. Al-Ama, Zh. Neorg. Khim. 46 (9) (2001) 1442–1448.
[2] J.-X. Mi, Y.-X. Huang, S.-Y. Mao, X.-D. Huang, Z.-B. Wei, Z.-L. Huang, J.-T. Zhao, J. Solid State Chem. 157 (2001) 213–219.
[3] A.A. Filaretov, M.G. Zhizhin, A.V. Olenev, A.A. Gurkin, A.P. Bobylev, B.I. Lazoryak, V.P. Danilov, L.N. Komissarova, Zh. Neorg. Khim. 47 (12) (2002) 1930–1946.
[4] S.-Y. Mao, M.R. Li, J.-X. Mi, H.-H. Chen, J.-F. Deng, J.-T. Zhao, Z. Kristallogr. 217 (2002) 311–312.
[5] Y.-X. Huang, M.-R. Li, J.-X. Mi, H.-H. Chen, J.-T. Zhao, Chin. J. Inorg. Chem. 20 (10) (2004) 1191–1196.
[6] J. Lesage, L. Adam, A. Guesdon, B. Raveau, J. Solid State Chem. 180 (2007) 1799–1808.
[7] R.C. Haushalter, Z.-W. Wang, M.E. Thompson, J. Zubieta, Inorg. Chim. Acta 232 (1995) 83–89.
[8] Z. Bircsak, W.T.A. Harrison, Acta Crystallogr. C54 (1998) 1195–1197.
[9] I. Vencato, E. Mattievich, L.F. Moreira, Y.P. Mascarenhas, Acta Crystallogr. C45 (1989) 367–371.
[10] O.V. Yakubovich, Kristallografiya 38 (5) (1993) 43–48.
[11] K.-H. Lii, L.-S. Wu, J. Chem. Soc., Dalton Trans. (1994) 1577–1580.
[12] S.M. Stalder, A.P. Wilkinson, J. Mater. Chem. 8 (1) (1998) 261–263.
[13] W. Yan, J. Yu, Z. Shi, R. Xu, Chem. Commun. (2000) 1431–1432.
[14] B. Ewald, Y.-M. Prots, H. Zhang, R. Kniep, Z. Kristallogr - New Cryst. Struct. 219 (2004) 343–344.
[15] Duisenberg, Kroon-Batenburg, Schreurs, J. Appl. Crystallogr. 36 (2003) 220.
[16] V. Pretricek, M. Dusek, The Crystallographic Computing System JANA2000, Institute of Physics, Praha, Czech Republic, 2000.
[17] N.E. Brese, M. O'Keeffe, Acta Crystallogr. B47 (1991) 192–197.
[18] G. Herzberg, Infrared and Raman Spectra of Polyatomic Molecules, ninth ed., vol. II, D. Van Nostrand Company, Inc., Princeton, 1960.
[19] M. Daturi, G. Busca, A. Guesdon, M.M. Borel, J. Math. Chem. 11 (2001) 1726–1731.
[20] V. Koleva, H. Effenberger, J. Solid State Chem. 180 (2007) 956–967.
[21] M.A. Strelkov, M.G. Zhizhin, L.N. Komisserova, J. Solid State Chem. 179 (2006) 3664–3671.
[22] M.P. Attfield, A.K. Cheetham, S. Natarajan, Mater. Res. Bull. 35 (2000) 1007–1015.
[23] C.E. Rice, W.R. Robinson, B.C. Tofield, Inorg. Chem. 15 (1976) 345–348.
[24] N. Middlemiss, C. Calvo, Acta Crystallogr. B32 (1976) 2896–2898.
[25] A. Leclaire, J. Chardon, A. Grandin, M.-M. Borel, B. Raveau, J. Solid State Chem. 108 (1994) 291–298.
[26] K.-H. Lii, Y.P. Wang, Y.B. Chen, S.-L. Wang, J. Solid State Chem. 86 (1990) 143–148.
[27] M.-R. Li, S.-Y. Mao, H.-H. Chen, J.-F. Deng, J.-X. Mi, J.-T. Zhao, Z. Kristallogr. 217 (2002) 309–310.
[28] P. Vasic, B. Prelesnik, M. Curic, R. Herak, Z. Kristallogr. 173 (1985) 193–198.
[29] M.-T. Averbuch-Pouchot, A. Durif, J.-C. Guitel, I. Tordjman, M. Laugt, Bull. Soc. Fr. Miner. Crystallogr. 96 (1973) 278–280.
[30] M.-T. Averbuch-Pouchot, J. Appl. Crystallogr. 7 (1974) 511–512.